ISIJ International, Vol. 39 (1999), No. 4, pp. 346–351

Evaluation of Heterogeneity in Thickness of Passive Films on Pure Iron by Scanning Electrochemical Microscopy

Koji FUSHIMI, Kazuhisa AZUMI and Masahiro SEO

Graduate School of Engineering, Hokkaido University, North 13, West 8, Kita-ku, Sapporo, Hokkaido, 060-8628 Japan.

(Received on September 10, 1998; accepted in final form on December 21, 1998)

Scanning electrochemical microscopy (SECM) was applied to evaluate the heterogeneity of a passive film formed on a pure iron electrode in deaerated pH 8.4 borate solution. A probe current image of SECM was measured with a tip-generation/substrate-collection (TG/SC) mode in deaerated pH 8.4 borate solution containing 0.03 mol dm^{-3} $Fe(CN)_6^{4-}$ as a mediator. The difference in thickness of passive films formed on two iron plates at different potentials could be evaluated from the probe current image. The probe current image of the passivated iron surface with distinctive crystal grains was composed of the patch patterns, the shapes of which coincided completely with the shapes of the substrate crystal grains. The probe current flowed above the grain surface oriented to {100} plane was less than that above the grain surface oriented to {110} or {111} plane. The grain orientation dependence of probe current was ascribed to the difference in thickness of passive films formed on the crystal grains.

KEY WORDS: scanning electrochemical microscopy; heterogeneity; passive film; film thickness; iron; grain orientation.

1. Introduction

Passive films formed on metals and alloys sustain corrosion resistivities of substrates. A local breakdown of passive film eventually leads to localized corrosion such as pitting. Measurements of electrochemical reactivities at the local sites of the passive film are important for better understanding of precursor processes of localized corrosion. Scanning electrochemical microscopy (SECM)[1,2] is useful and powerful technique for an *in-situ* evaluation of electrochemical reactivities at the local sites. SECM has been applied so far to many fields including microelectrochemistry,[2-6] bioelectrochemistry,[7-9] microfabrication[10-12] and so on.

Bard *et al.* used SECM to examine surface oxide films on chromium[13] and on titanium[14] and showed that these oxide films have insulative properties. Smyrl *et al.* investigated the precursor processes of pitting corrosion of titanium[15-19] by SECM. Wipf *et al.* also employed SECM to investigate the breakdown of passive films on stainless steel[20] and iron.[21] Although these studies by SECM provided the first step for investigating the precursor processes of pitting, the heterogeneity of thickness or defective structure of a passive film, which would be directly related to the local breakdown, has not been well evaluated.

In this study, SECM was applied to a passive film formed on a pure iron and the heterogeneity of the passive film was examined from the difference in activity of redox reaction which takes place on the passive iron surface.

2. Experimental

2.1. SECM

A block diagram of the apparatus used for SECM experiments is shown in **Fig. 1**. A probe electrode is located just above a specimen electrode and it can detect the change in activity of a redox reaction on the specimen electrode as a probe current. If the distance (z axis) between the probe and specimen electrodes is kept constant and the probe electrode is scanned in the directions of x and y axes, the probe current images are obtained, from which the heterogeneity of the specimen surface would be evaluated.

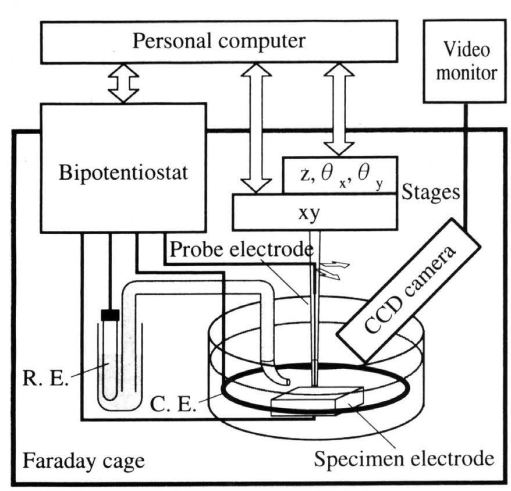

Fig. 1. Block diagram of the apparatus used for SECM experiments.

A dual axes positioner with controller (Seiko Instr., SP-2200 and SP-4200) and three micro-positioners with controller (Chuo Precision Indust., AME-15 and M9103) were used for scanning (x and y axes) and positioning (z, θ_x and θ_y axes) the probe electrode, respectively. The probe electrode can be controlled with accuracies of 0.01 μm step^{-1} in the x or y direction, of 0.1 μm step^{-1} in the z direction, and of about 2×10^{-9} degree step^{-1} in the tilting (both θ_x and θ_y). The potential, E_p, of probe electrode and the potential, E_s, of specimen electrode were controlled independently with a bipotentiostat (Hokuto Denko Co.) specially built for SECM. A silver–silver chloride electrode and a platinum plate were used as a reference electrode and a counter electrode, respectively, and all potentials were converted to a standard hydrogen electrode (SHE). The current, I_p, of probe electrode and the current, I_s, of specimen electrode were simultaneously measured as a function of the position of the probe electrode. Five dimensional (x, y, z, θ_x, and θ_y) and four electrochemical (E_p, E_s, I_p, and I_s) parameters were controlled and recorded with a personal computer.

2.2. Specimen Preparation and Experimental Set up

The probe electrode was a disc-shaped microelectrode composed of a platinum wire with a diameter of 10 μm which was thermally sealed into a glass capillary. The tip of the probe electrode was mechanically polished with a diamond whetstone (#5000) on a turntable (Narishige Co., EG-400). For cleaning, cyclic voltammetry of the probe electrode was performed in the potential region between hydrogen evolution and oxygen evolution in 1 mol dm^{-3} sulfuric acid until the same voltammograms were obtained.

The iron specimen used in experiments was a polycrystalline iron plate with a purity above 99.99%. The surface preparation of the iron specimen depending on the aim of the research, was performed with the following two different procedures, I and II.

I: the iron specimen was mechanically polished with alumina abrasives down to a size of 0.05 μm, rinsed with doubly distilled water and finally dried with purified nitrogen gas.

II: after mechanical polishing with the above procedure, the iron specimen was subjected to chemical etching in ethanol solution containing 10 vol% nitric acid for 15 s to remove the Beilby layer, rinsed with doubly distilled water and finally dried with purified nitrogen gas.

The two iron plates (200 μm × 5 mm × 10 mm) prepared with the procedure I were embedded into epoxy resin as shown in **Fig. 2**. The cross section (200 μm × 5 mm) of each plate was mechanically polished again with alumina abrasives. This type of iron electrode was employed to examine the difference in thickness of passive films formed on two iron plates at different potentials. On the other hand, the iron plate (1.5 mm × 7.5 mm × 10 mm) prepared with the procedure II was mounted on a specimen holder covered with epoxy resin and the surface area (7.5 mm × 10 mm) of the plate as prepared was exposed to environment. The latter type of iron electrode was employed to examine the heterogeneity of passive films depending on the grain orientation of the iron substrate because the procedure II can make distinctive each crystal grain on the substrate iron surface.

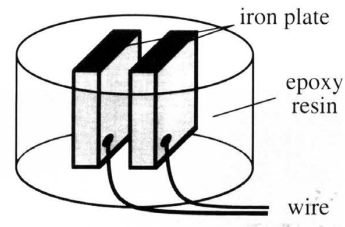

Fig. 2. Specimen electrode with two iron plates embedded into epoxy resin.

Both types of iron electrodes were cathodically polarized in deaerated pH 6.5 borate solution under a constant current density of 5 μA cm^{-2} to remove an air-formed oxide film. After the cathodic polarization, the iron electrodes were potentiostatically passivated for 1 h in deaerated pH 8.4 borate solution to form passive films. $K_4Fe(CN)_6$ was employed as a mediator of the redox reaction taking place on the passivated iron. After the passivation, deaerated pH 8.4 borate solution containing 0.03 mol dm^{-3} $K_4Fe(CN)_6$ was introduced into the SECM cell and then the potentials of probe and iron electrodes were controlled at $E_p=1.2$ V and $E_s=0.1$ V, respectively with the bipotentiostat. In this potential condition, the oxidation of $Fe(CN)_6^{4-}$ proceeds on the probe electrode at $E_p=1.2$ V, whereas the reduction of $Fe(CN)_6^{3-}$ produced on the probe electrode proceeds on the iron electrode at $E_s=0.1$ V. It is known that the flat band potential, E_{fb}, of the passive film on iron is -0.16 V in pH 8.4 borate solution.[22] The passive film on iron in the solution may be cathodically reduced at potentials lower than E_{fb}. Therefore, $E_s=0.1$ V higher than E_{fb} was chosen to avoid the changes in thickness of the passive film during the measurement of probe current image.

If the distance between probe and specimen electrodes is short enough within the length of diffusion layer of $Fe(CN)_6^{4-}$ or $Fe(CN)_6^{3-}$ on the probe electrode in bulk solution, the oxidation of $Fe(CN)_6^{4-}$ on the probe electrode is enhanced or retarded just above the local sites of iron surface with a high or low reactivity of reduction of $Fe(CN)_6^{3-}$ due to a spatial limitation of diffusion as described later. The above mode in which probe current image is measured, is called "tip-generation/substrate-collection (TG/SC) mode" according to Bard *et al.*[23,24] In this experiment, the distance between probe and specimen electrodes, $d_{s,p}$, is so controlled as to the value of probe current being about 0.6 times as much as that of the limiting current measured when the probe electrode is located more than 200 μm far from the specimen electrode. According to our previous SECM study[25] in which a model specimen electrode with platinum foil and wire embedded into epoxy resin was used, the lateral resolution of the probe current image measured at the above electrochemical and geometrical conditions was about two times as much as the diameter of probe electrode as shown in **Fig. 3**.

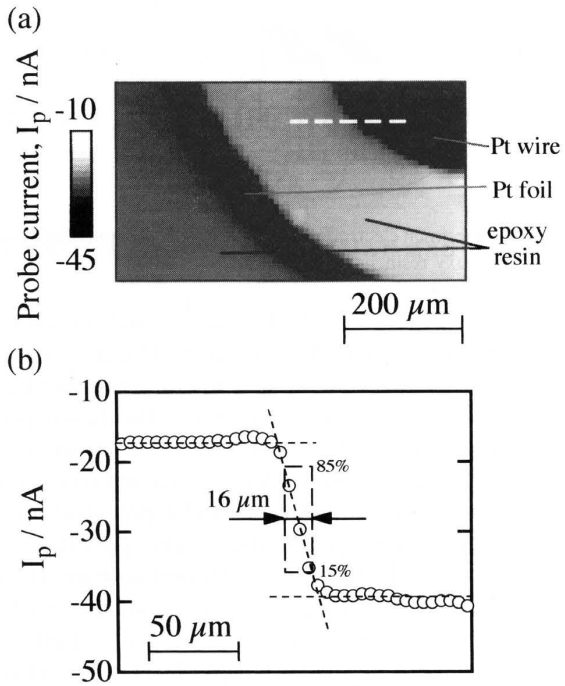

Fig. 3. (a) Probe current image obtained when the probe electrode with a diameter of 10 μm was scanned over the model specimen electrode surface. The probe electrode and Pt wire in the model electrode were polarized at −0.1 and 0.9 V (SHE), respectively, whereas the Pt foil in the specimen electrode was in an open circuit, in deaerated pH 8.4 borate solution containing 0.03 mol dm^{-3} $K_4Fe(CN)_6$.
(b) Probe current profile obtained when the probe electrode was scanned along the dashed line drawn on the current image. The lateral resolution of the probe current image estimated from the probe current profile at the boundary of Pt wire and epoxy resin was 16 μm, which was two times as much as the diameter of probe electrode.

2.3. Observation of the Specimen Surface

A surface roughness of the iron specimen subjected to chemical etching was measured by a surface profilometer (Tokyo Seimitsu Co., Surfcom) equipped with a diamond tip (a diameter of 0.01 μm) for surface tracing. After the measurement of a probe current image, an optical micrograph of the same region was taken for comparison with the probe current image. Furthermore, the orientation of each crystal grain on the substrate iron surface was examined by an etch-pit method. Three different kinds of solutions (a), (b), and (c) as described in **Table 1** were prepared for an etch-pit method. The iron specimen was immersed into these solutions in the following order: solution (a) for 10 s → solution (b) for 50 s → solution (c) for 10 s → solution (b) for 30 s. After every immersion, the iron specimen was rinsed with doubly distilled water. This etching treatment provides the shape of the pit depending on the orientation of each grain. Each pit is mainly composed of low index planes ({100} and {110}) of a polyhedron[26,27]. The shape of each pit was confirmed with SEM observations, from which the orientation of the grain was evaluated.

Table 1. Solutions (a), (b), and (c) prepared for an etch-pit method.

	Chemicals	(Thier mixing ratios in volume)
(a)	$HCl:H_2O_2:H_2O$	(1:10:100)
(b)	sat. $FeCl_3$ aq. sol.: $HNO_3:H_2O$	(2:1:10)
(c)	$HCOOH:H_2O_2:C_2H_5OH:H_2O$	(1:1:1:1)

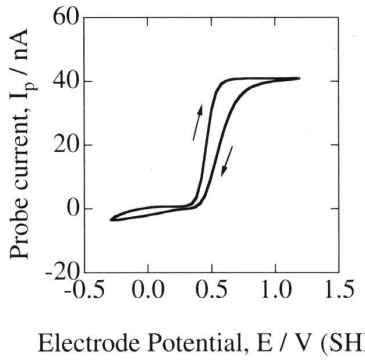

Fig. 4. Cyclic voltammogram of the probe electrode measured in deaerated pH 8.4 borate solution containing 0.03 mol dm^{-3} $Fe(CN)_6^{4-}$ when the probe electrode is far from the specimen electrode. The potential sweep rate was 100 mV s^{-1}.

3. Results and Discussion

3.1. Characteristics of Probe Electrode

Figure 4 shows the cyclic voltammogram of the probe electrode measured in deaerated pH 8.4 borate solution containing 0.03 mol dm^{-3} $Fe(CN)_6^{4-}$ when the probe electrode is far from the specimen electrode. The cyclic voltammogram has a sigmoid shape with a limiting current, $I_{p,l}=41$ nA at potentials above 0.6 V. This limiting current is in a good agreement with that derived theroretically for a disc microelectrode with a hemispherical diffusion layer. The theoretical limiting current, $I_{p,l}$, can be described as follows.[28]

$$I_{p,l}=4nFDCa \quad \text{.....(1)}$$

where D and C are the diffusion coefficient and the concentration of mediator, respectively, a is the diameter of probe electrode, n is the number of electrons participating in the redox reaction, and F is the Faraday constant. When the probe electrode approaches to the specimen electrode within a distance corresponding to the length of diffusion layer, the probe current, I_p, changes depending on electronic properties of the specimen electrode surface due to a spatial limitation of diffusion.[29,30] In case where the specimen electrode surface is insulative, the probe current, I_p, decreases with decreasing the distance, $d_{s,p}$, because the reduction of $Fe(CN)_6^{3-}$ occurs scarcely on the insulative surface and the supply of $Fe(CN)_6^{4-}$ from the outside is spatially limited, that is, the probe electrode is subjected to a negative feedback condition. On the other hand, in case where the specimen electrode surface is a good electronic conductor, the probe current, I_p, increases with decreasing the distance, $d_{s,p}$, because the reduction of $Fe(CN)_6^{3-}$ proceeds easily on the electroconductive surface and the transport of $Fe(CN)_6^{4-}$ to the outside is spatially limited, that is, the probe electrode is subjected

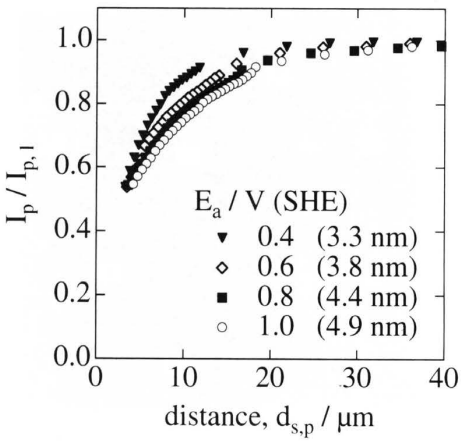

Fig. 5. Normalized probe current, $I_p/I_{p,l}$, as a function of the distance, $d_{s,p}$, between probe and iron electrodes. The probe and iron electrodes were polarized at 1.2 and 0.1 V (SHE), respectively, in deaerated pH 8.4 borate solution containing 0.03 mol dm^{-3} $K_4Fe(CN)_6$, after the iron electrode was passivated at $E_a = 0.4$, 0.6, 0.8 or 1.0 V (SHE) for 1 h in deaerated pH 8.4 borate solution. The numerical value in parenthesis represents the thickness of passive film[33] formed at E_a.

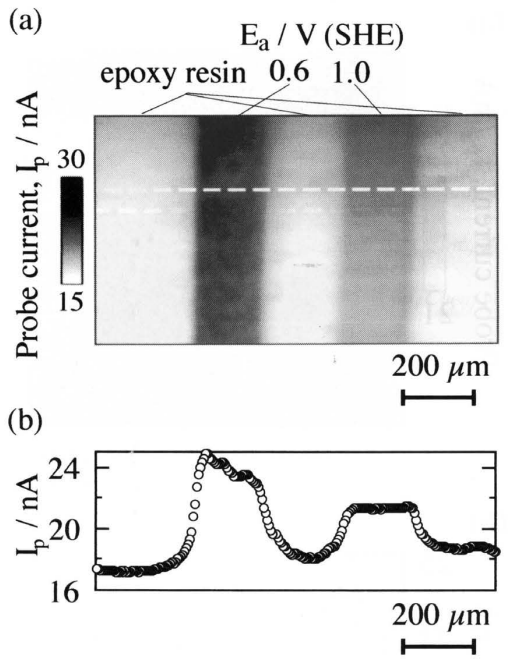

Fig. 6. (a) Probe current image of the specimen electrode with two iron plates embedded into epoxy resin. The two iron plates were anodically polarized at $E_a = 0.6$ and 1.0 V (SHE) for 1 h to form the passive films[33] with different thickness (3.8 and 4.9 nm), respectively, prior to the measurement of the probe current image. For the measurement of the probe current image, the probe and iron electrodes were polarized at 1.2 and 0.1 V (SHE), respectively, in deaerated pH 8.4 borate solution containing 0.03 mol dm^{-3} $K_4Fe(CN)_6$.
(b) Probe current profile along the dashed line drawn in Fig. 6(a).

to a positive feedback condition.

3.2. Normalized Probe Current as a Function of the Distance between Probe and Iron Electrodes

After the iron electrode was passivated at $E_a = 0.4$, 0.6, 0.8 or 1.0 V for 1 h in deaerated pH 8.4 borate solution, the probe current, I_p, was measured at $E_p = 1.2$ V and $E_s = 0.1$ V in deaerated pH 8.4 borate solution containing 0.03 mol dm^{-3} $K_4Fe(CN)_6$ as a function of the distance between probe and iron electrodes, $d_{s,p}$. In **Fig. 5**, the probe current normalized with a limiting probe current, $I_p/I_{p,l}$, was plotted *vs.* $d_{s,p}$. The value of $I_p/I_{p,l}$ decreases with decreasing $d_{s,p}$, indicating that the passive iron surface is semiconductive or insulative. Moreover, at $d_{s,p}$ less than 15 μm, the value of $I_p/I_{p,l}$ decreases with increasing E_a.

It is known that the passive film on iron has a semiconductive property[31,32] of n type with a band gap energy of 1.6–2.0 eV. The ellipsometrical results[33] indicated that the thickness of passive films formed on iron in pH 8.4 borate solution increased linearly from 1 to 5 nm with increasing the potential of film formation, E_a. A transfer reaction of electrons between passive metal substrate and redox system in solution proceeds with a direct tunneling of electrons across the passive film, if the Fermi level of redox system is located in the forbidden band of the film and the film thickness is small enough (less than 3 nm) for tunneling. In this case, it is theoretically derived that the tunneling probability decreases exponentially with increasing the film thickness.

The decrease in $I_p/I_{p,l}$ with increasing E_a, *i.e.*, the film thickness, at $d_{s,p}$ less than 15 μm in Fig. 5 reflects on the redox reactivity of the passive iron surface. In principle, therefore, the probe current image which is measured by scanning the probe electrode in the direction of x and y axes at $d_{s,p} = 5$ μm corresponding to $I_p/I_{p,l} = 0.6$ can evaluate the difference in thickness of passive films on iron. Schultze *et al.*[34] found that the redox current of $Fe(CN)_6^{4-}$ and $Fe(CN)_6^{3-}$ on iron electrode passivated in pH 8.4 borate solution decreased with increasing the film thickness. The results of Fig. 5 are consistent with those by Schultze *et al.*[34]

3.3. Evaluation of the Difference in Thickness of Passive Film from Probe Current Image

Figure 6(a) shows the probe current image of the specimen electrode with two iron plates separated with epoxy resin. The two iron plates were anodically polarized at $E_a = 0.6$ and 1.0 V for 1 h to form the passive films[33] with different thickness (3.8 and 4.9 nm), respectively, prior to the measurement of the probe current image. It is seen from Fig. 6(a) that the probe current flowed above the epoxy resin surface is relatively low compared with that above the iron plate surface, because the epoxy resin surface is insulative. Moreover, it is noticed that the higher probe current flows above the iron plate surface covered with the thinner passive film, proving that the difference in thickness of passive films on iron can be evaluated from the probe current image. **Figure 6(b)** shows the probe current profile along the dashed line drawn in Fig. 6(a). The line profile of probe current above the iron plate surface covered with thicker passive film (4.9 nm) are rather smooth, indicating that the passive film formed at 1.0 V is more uniform than that formed at 0.6 V. The lateral resolution of the probe current image was

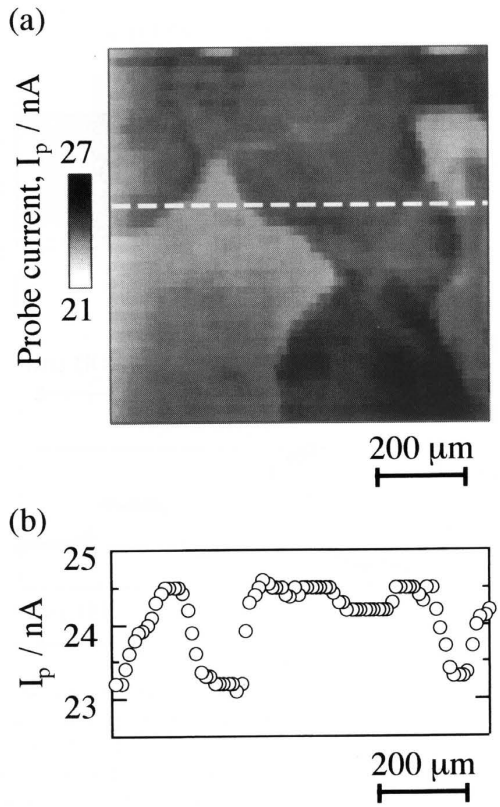

Fig. 7. (a) Probe current image measured after the iron electrode surface with distinctive crystal grains was passivated at 1.0 V (SHE) for 1 h. For the measurement of the probe current image, the probe and iron electrodes were polarized at 1.2 and 0.1 V (SHE), respectively, in deaerated pH 8.4 borate solution containing 0.03 mol dm^{-3} $K_4Fe(CN)_6$.
(b) Probe current profile along the dashed line drawn in Fig. 7(a).

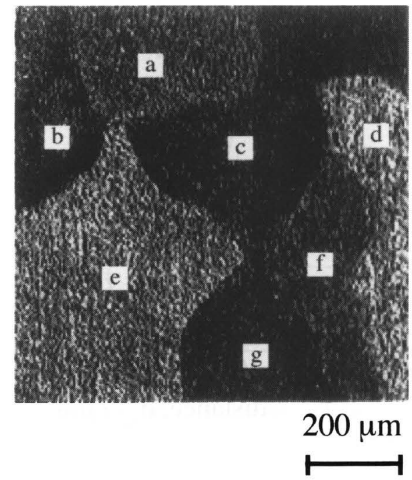

	Index plane	rotation angle	
		[100]	[010]
a	$(\bar{0}11)$	-10°	5°
b	(111)	0°	-5°
c	(101)	-5°	15°
d	(001)	10°	0°
e	$(0\bar{0}1)$	10°	0°
f	$(\bar{1}01)$	-10°	5°
g	(101)	0°	15°

Fig. 8. Optical micrograph of the same surface region where the probe current image was measured. The index planes described on the optical micrograph represent the orientation of each crystal grain evaluated from the shape of the etch pit. The real deviation from the index plane is described by rotation angles about [100] and [010] axes in the table.

estimated to be 23 μm from the probe current profile at the boundary between epoxy resin and iron plate with passive film formed at 1.0 V, which was slightly larger than two times as much as a diameter of the probe electrode.

3.4. Heterogeneity of the Passive Film Associated with Orientation of the Substrate Crystal Grain

Figure 7(a) shows the probe current image measured after the iron electrode surface with distinctive crystal grains was passivated at 1.0 V for 1 h. The probe current profile along the dashed line drawn in Fig. 7(a) is also shown in **Fig. 7(b)**. Moreover, **Figure 8** shows the optical micrograph of the same surface region where the probe current image was measured. The index planes described on the optical micrograph represent the orientation of each crystal grain evaluated from the shape of the etch pit. It is seen from the comparison between Figs. 7(a) and 8 that the shapes of patch patterns on the probe current image coincide completely with the shapes of crystal grains on the iron surface. Furthermore, the probe current flowed above the grain surface oriented to {100} plane is less than that above the grain surface oriented to {110} or {111} plane. At first, the surface roughness of the iron surface has to be taken into consideration to explain the grain orientation dependence of the probe current. The measured surface roughness profile indicated that the {100} grain surface is concave, while the {110} or {111} grain surface is convex, and the height difference at the boundary between the {100} and {110} grains is about 0.4 μm. Assuming the same redox reactivities of the {100} and {110} grains, the change in probe current between {100} and {110} grains originated only from the geometry can be easily estimated using the normalized probe current *vs.* distance curve at $E_a =$ 1.0 V in Fig. 5. The estimated change in probe current corresponding to the height difference of 0.4 μm at the grain boundary is 0.6 nA. On the other hand, the real change in probe current at the grain boundary obtained from Fig. 7(b) is 1.4 nA which is 2.3 times as much as the estimated value. The change of 0.8 nA in probe current at the boundary between {110} and {100} crystal grains still remains even if the correction of probe current is made for the height difference at the grain boundary. This result argues that the difference in thickness of passive films formed on the {110} and {100} crystal grains would reflect on the probe current image of Fig. 7(a) or probe current profile of Fig. 7(b). It is expected that the passive film formed on the {110} grain is thinner than that on the {100} grain since the probe current above the {110} grain is larger than that above the {100} grain.

Kudelka *et al.*[35] measured the thickness of passive films formed on a polycrystalline titanium electrode by an anisotropy micro-ellipsometry[36] and found that the passive film formed on the (0001) grain with the high

packing density of the substrate surface is thinner than that on the (xxx0) grain with the low packing density. In case of iron, the packing density of the {110} grain surface is higher than that of the {100} grain surface. The similar relation between the thickness of the passive film and the packing density of the substrate grain may hold for iron as well as titanium. The reason why the thinner passive film is formed on the substrate grain with the higher packing density is not well understood, although it is probable that the high packing density hinders the penetration of the electric field into the metal surface and suppresses the passive film growth.[35] We need further experiments to confirm the dependence of passive film thickness on the orientation of the substrate iron grains.

4. Conclusions

SECM was applied to evaluate the heterogeneity of passive film formed on a polycrystalline iron electrode in deaerated pH 8.4 borate solution. The following conclusions were drawn.

(1) The difference in thickness of passive films formed on two iron plates at different potentials could be evaluated from the probe current image measured in deaerated pH 8.4 borate solution containing $Fe(CN)_6^{4-}$ as a mediator.

(2) The shapes of the patch patterns on the probe current image coincided completely with the shapes of crystal grains on the substrate iron surface.

(3) The probe current flowed above the grain surface oriented to {100} plane was less than that above the grain surface oriented to {110} or {111} plane.

(4) The grain orientation dependence of probe current was ascribed to the difference in thickness of passive films formed on the crystal grains.

Acknowledgments

This research was supported by the Monbusho (Ministry of Education, Science, Culture and Sports of Japan) Grant-in-Aid for Scientific Research (No. 08555166) and the ISIJ (Iron and Steel Institute of Japan) Research Promotion Grant. The authors are indebted to Prof. W. H. Smyrl and Dr. P. James (University of Minnesota, USA) for their helpful comments of construction of SECM, to Prof. Y. Ito (Hokkaido University) for his comment of the etch-pit method, and to Mr. M. Matsudaira, Mr. A. Hukuizumi, and Dr. E. Fujimoto (Hokuto Denko Co.) for their design of the bipotentiostat.

REFERENCES

1) A. J. Bard, F.-R. F. Fan, J. Kwak and O. Lee: *Anal. Chem.*, **61** (1989), 132.
2) A. J. Bard, F.-R. F. Fan, D. Pierce, P. R. Unwin, D. O. Wipf and F. Zhou: *Science*, **254** (1991), 68.
3) R. C. Engstrom, M. Weber, D. J. Wunder, R. Burgess and S. Winquist: *Anal. Chem.*, **58** (1986), 844.
4) A. J. Bard, G. Denuault, R. A. Friesner, B. C. Dornblaser and L. S. Tuckerman: *Anal. Chem.*, **63** (1991), 1282.
5) P. R. Unwin and A. J. Bard: *J. Phys. Chem.*, **95** (1991), 7814.
6) Y.-F. Yang and G. Denuault: *J. Chem. Soc. Faraday Trans.*, **92** (1996), 3791.
7) J. Wang, L.-H. Wu and R. Li: *J. Electroanal. Chem.*, **272** (1989), 285.
8) D. T. Pierce, P. R. Unwin and A. J. Bard: *Anal, Chem.*, **64** (1992), 1795.
9) B. R. Horrocks, D. Schmidtke, A. Heller and A. J. Bard: *Anal. Chem.*, **65** (1993), 3605.
10) O. E. Husser, D. H. Craston and A. J. Bard: *J. Electrochem. Soc.*, **136** (1989), 3222.
11) D. Mandler and A. J. Bard: *J. Electrochem. Soc.*, **137** (1990), 1079.
12) D. Mandler and A. J. Bard: *J. Electrochem. Soc.*, **137** (1990), 2468.
13) C. Lee and A. J. Bard: *Anal. Chem.*, **62** (1990), 1906.
14) C. Wei and A. J. Bard: *J. Electrochem. Soc.*, **142** (1995), 2523.
15) N. Casillas, S. Charebois, W. H. Smyrl and H. S. White: *J. Electrochem. Soc.*, **140** (1993), L142.
16) N. Casillas, P. James and W. H. Smyrl: *J. Electrochem. Soc.*, **142** (1995), L16.
17) N. Casillas, S. Charebois, W. H. Smyrl and H. S. White: *J. Electrochem. Soc.*, **141** (1994), 636.
18) J. P. H. Sukamto, W. H. Smyrl, N. Casillas, M. A.-Odan, P. James, W. Jin and L. Douglas: *Mater. Sci. Eng. A*, **198** (1995), 177.
19) P. James, N. Casillas and W. H. Smyrl: *J. Electrochem. Soc.*, **143** (1989), 3853.
20) D. O. Wipf: *Coll. Surf. A: Phys. Eng. Asp.*, **93** (1994), 251.
21) J. W. Still and D. O. Wipf: *J. Electrochem. Soc.*, **144** (1997), 2657.
22) K. Azumi, T. Ohtsuka and N. Sato: *J. Electrochem. Soc.*, **134** (1987), 1352.
23) C. Lee, J. Kwak and F. C. Anson: *Anal. Chem.*, **63** (1991), 1501.
24) F. Zhou, P. R. Unwin and A. J. Bard: *J. Phys. Chem.*, **96** (1992), 4917.
25) K. Fushimi and M. Seo: *Zairyo-to-Kankyo*, **46** (1997), 797.
26) H. Hayakawa and J. Imamura: *Bull. Jpn. Inst. Met.*, **18** (1979), 282.
27) Y. Kinoshita and S. Takeda: *Bull. Jpn. Inst. Met.*, **18** (1979), 642.
28) Y. Saito: *Rev. Polarogr. Jpn.*, **15** (1968), 177.
29) J. Kwak and A. J. Bard: *Anal. Chem.*, **61** (1989), 1221.
30) A. J. Bard, F.-R. F. Fan and M. V. Mirkin: "Electroanalytical Chemistry", Vol. 18, ed. by A. J. Bard, Marcel Dekker, Inc., New York, (1994), 243.
31) J. W. Schultze and U. Stimming: *Ber. Bunsenges. Phys. Chem.*, **80** (1976), 1297.
32) S. M. Wilhelm, K. S. Yun, L. W. Ballenger and H. Hackerman: *J. Electrochem. Soc.*, **126** (1979), 419.
33) N. Sato, T. Noda and K. Kudo: *Electrochim. Acta*, **19** (1974), 471.
34) J. W. Schultze and U. Stimming: *Z. Phys. Chem. N. F.*, **98** (1975), 285.
35) S. Kudelka and J. W. Schultze: *Electrochim. Acta*, **42** (1997), 2817.
36) A. Michaelis and J. W. Schultze: *Thin Solid Films*, **233** (1993), 86.